Auditory processing in the brainstem and audiovisual integration in humans studied with fMRI

Slabu, Lavinia Mihaela

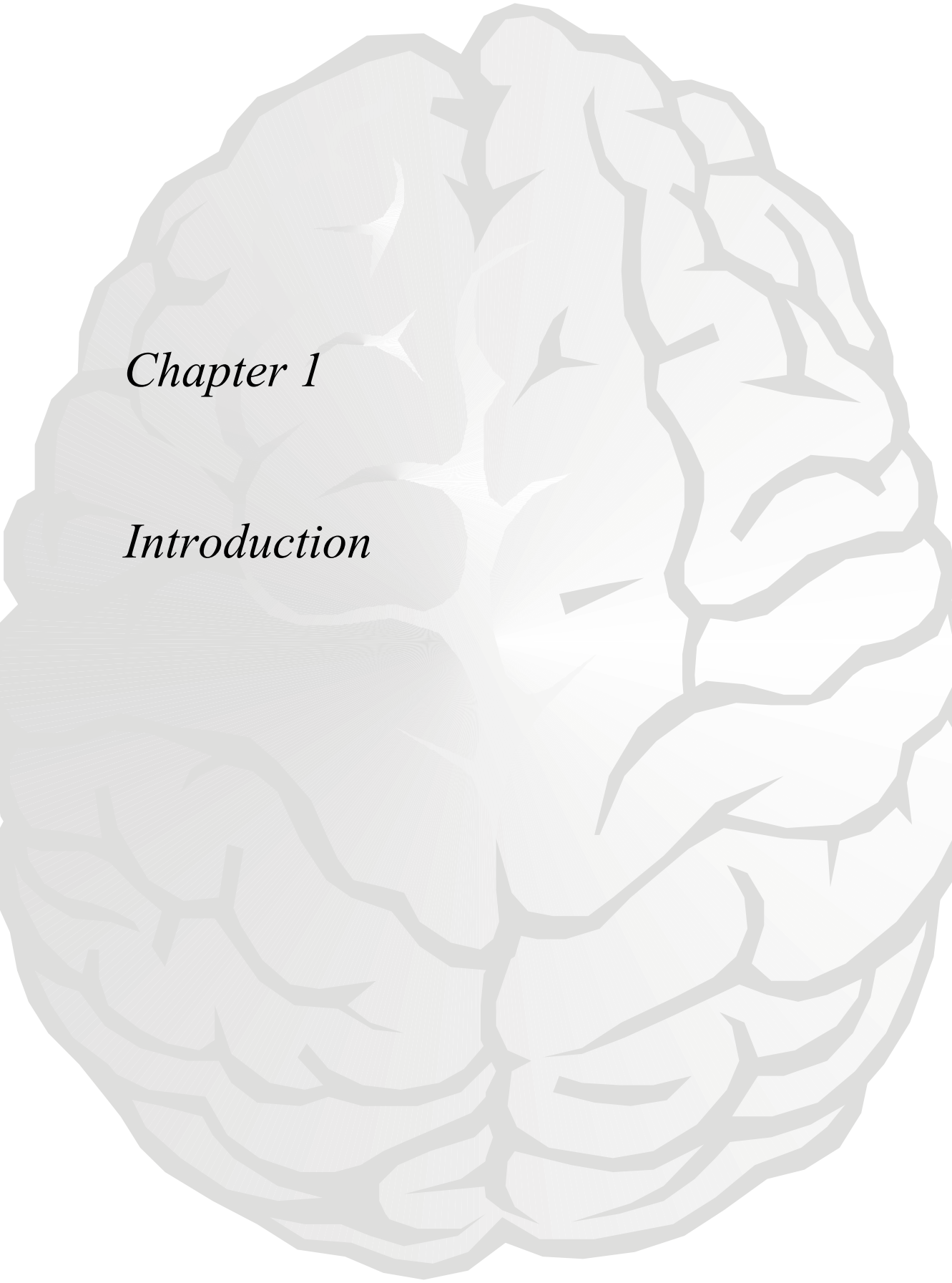

Chapter 1

Introduction

1.1. Outline

This thesis discusses the application of functional magnetic resonance imaging (fMRI) to the auditory system in the human brain. The main goal of this research is a better understanding of the auditory subcortical mechanisms.

Chapter 2 describes recent fMRI/MRI studies on the human central auditory pathway, emphasizing anatomical, methodological, technical issues, and applications to the brainstem.

Chapters 3 and 4 describe the effects of slice orientation on the inferior colliculi, superior olivary complex, and cochlear nucleus. Using fMRI we detect differences on the activation cluster for the inferior colliculi. Our results indicate that the imaging plane at 45 degrees to the brainstem has the lowest sensitivity to motion (reflected in the standard deviation and normalized standard deviation) and offers the highest spatial accuracy for the inferior colliculi and auditory cortex. The orthogonal slice orientation offers the highest effect size but with a reduced spatial specificity.

Chapter 5 describes experiments on audiovisual integration in speech perception. These address the sensitivity of subjects for certain combination of audio-visual speech stimulus information [Tomaskovic, 2006].

The first chapter briefly introduces concepts that are used in the thesis: physical principles of MRI, fMRI and Blood Oxygen Level Dependant (BOLD) signal, auditory and visual processing, and a brief description of brain anatomy.

1.2. Physical principles of MRI

The major noninvasiveness neuroimaging techniques are positron emission tomography (PET), single photon emission computed tomography (SPECT), computer tomography (CT), magnetic resonance imaging (MRI), magnetoencephalography (MEG), electroencephalography (EEG), and, ultrasound (US) [see table 1.1].

Magnetic resonance imaging (MRI) is a non-invasive technique of obtaining clinical images and of studying tissue metabolism in vivo. MRI involves nuclei (of an object to be imaged), magnetic fields, and the resonance phenomenon (arising from the interactions of the nuclei with the magnetic fields) [Liang and Lauterbur, 2000].

When a human body is placed in a large magnetic field, many of the free hydrogen nuclei from the soft body tissue align themselves with the direction of the magnetic field and create a net magnetic moment $(\overrightarrow{M})$ parallel to the magnetic field [see fig.1.1 A, B]. This behavior is associated with a precession of its nuclear spin around the external field and is termed Larmor precession.

Table 1.1. The characteristics for the methods of SPECT, CT, MRI, fMRI, MEG, and EEG [Churchland and Sejnowski, 1988; Casey and de Haan, 2002].

Characteristics	*Less* ⟶ *More*				
Ability to measure both cortical and deep structures			*MEG*	*SPECT CT*	*PET, fMRI*
Temporal resolution			*MRI PET SPECT*	*fMRI*	*EEG, MEG*
Spatial resolution	*EEG*	*MEG*	*SPECT*	*PET*	*fMRI, MRI CT*
Ease of use with developmental populations	*PET, SPECT*		*fMRI*	*MRI*	*EEG*

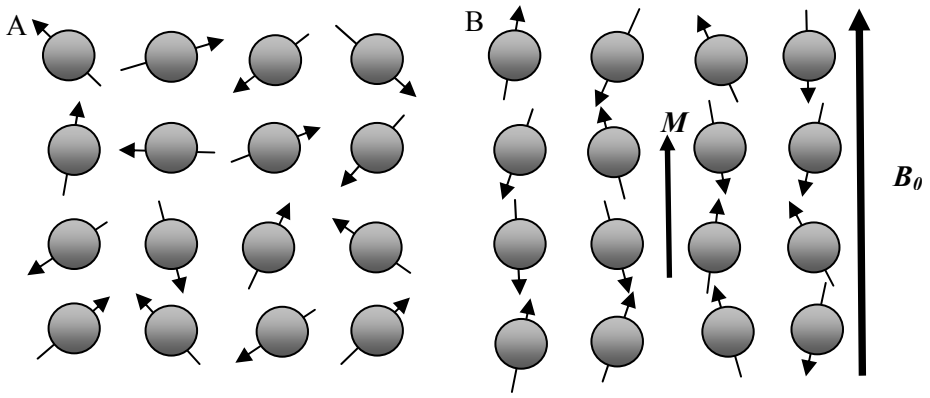

Figure 1.1. In the absence of a strong magnetic field, hydrogen nuclei are randomly aligned (A). When the strong magnetic field, B_0, is applied, the hydrogen nuclei precess about the direction of the field (B).

The frequency of Larmor precession is proportional to the applied magnetic field strength as defined by the Larmor frequency, ω_0:

$$\omega_0 = \gamma B_0 \tag{1.1}$$

where γ is the gyromagnetic ratio, a nuclei specific constant (for hydrogen, $\gamma = 42.6$ MHz/T), and B_0 is the strength of the applied magnetic field. The magnetic moments or spins are parallel and anti-parallel to B_0. The spin axes form an angle with B_0 and they precess around B_0 with Larmor frequency [see fig.1.1 B].

When a radio-frequency (RF) pulse with a frequency equal to the Larmor frequency, is applied perpendicular to B_0, the net magnetization, $\vec{M}$, is tilted into the transverse (xy-) plane. The angle through which $\vec{M}$ has rotated away from the z-axis is known as the flip angle [see fig.1.2].

When $\overrightarrow{M}$ has been tilted and RF field has been turned off, the magnetic moments of the protons will again rotate around the B_0. The signal due to this rotating magnetic field can be detected using a receiver coil.

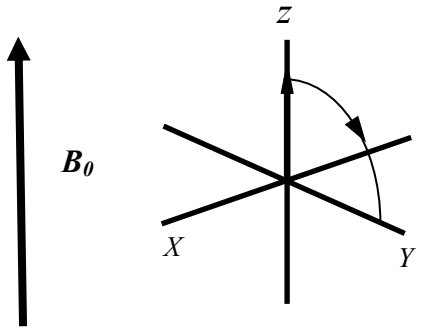

Figure 1.2. The effect of RF pulse

The return of $\overrightarrow{M}$ to its equilibrium state, to the direction of the z-axis, is known as relaxation and it is influenced by three factors: longitudinal *T1* or spin-lattice relaxation, transverse *T2* or spin-spin relaxation, and magnetic field inhomogeneity. During the relaxation processes both longitudinal and transverse components of the net magnetization return to their equilibrium values. The longitudinal component decays by a *T1* relaxation time. *T1* is a property of a tissue. Nuclei that were flipped to high energy states by an excitation pulse, transfer energy to the lattice in the process of returning to the lower state. At the same time transverse magnetization decays due to spin-spin dephasing and is described by a *T2* relaxation time. For brain tissue *T1* is approximately 1 s, and *T2* is approximately 0.1 s [Haacke et al., 1999]. Furthermore, spin coherence is affected by inhomogeneities in the applied magnetic field. The exponential decay in the signal resulting from the combination of *T2* relaxation and field inhomogeneities is referred to as *T2** - the effective transverse relaxation time. The effects of blood oxygen level on *T2** in MR were described by Seiji Ogawa in 1990 [Ogawa et al., 1990]: the cortical blood vessels were more visible as blood oxygen was lowered.

1.3. Functional magnetic resonance imaging

The ability to observe which structures participate in specific functions is due to a technique called functional magnetic resonance imaging (fMRI). This technique provides high resolution, noninvasive reports of neural activity detected by a blood oxygen level dependent (BOLD) signal [Ogawa et al., 1990, 1992, 1993, Belliveau et al., 1990, 1991].

fMRI is based on the increase in blood flow to the local vasculature that accompanies neural activity in the brain. The synaptic activity in neurons is accompanied by increased energy consumption and an increase in the cerebral metabolic rate of oxygen, and so the ratio of oxy/deoxy-hemoglobin will increase. Since magnetic susceptibility with surrounding tissue is affected, the decrease of deoxyhemoglobin alters the $T2^*$ weighted magnetic resonance image signal [Ogawa et al., 1990, 1992, 1993, Belliveau et al., 1990, 1991, Turner et al., 1991, Tank et al., 1992].

Thus, deoxyhemoglobin is sometimes referred to as an endogenous contrast enhancing agent, and serves as the source of the signal for fMRI [Bandettini et al., 1992, 1993]. In short, a diagram of BOLD effect is presented in fig. 1.3.

Presently, there are some undesirable aspects in the auditory fMRI studies that are connected to the high-level sound produced by the scanner and annexes. The 3 Tesla scanners produce sound pressure levels up to approximately 130 dB SPL [Hoiting, 2005]. The sound sources in the scanner room vary due to different causes, like air-handling system, liquid helium pump, electric current leads, Eddy currents and gradient coil noise [Ravicz et al., 2000].

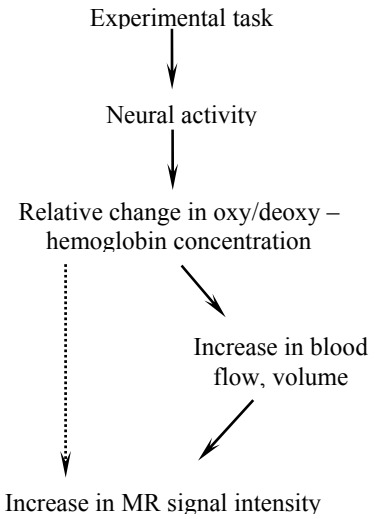

Figure 1.3. A diagram with events of BOLD

In practice, for the auditory experiments it is common that earmuffs and earplugs are worn. Moreover, a technique called "sparse" temporal sampling is used, where the volumes of brain images are acquired after the stimulus or rest conditions. To optimize detection of the activation, brain images are taken near the maxima and minima of the hemodynamic response during the experimental cycle [Hall et al., 1999, Renken, 2004]. The noise from the scanner can mask the stimuli [Shah et al., 2000, Eden et al., 1999] and induce brain activity that is not related to

the stimuli [Bandettini et al., 1998, Ulmer et al., 1998, Talavage et al., 1999, Edmister et al., 1999, Ravicz et al., 2000]. To avoid masking by the scanner noise, stimulus presentation should not overlap with volume acquisition starting 2 ms before and ending 200 ms after a volume acquisition [Duifhuis, 1973]. All experiments reported in this thesis were performed with a 3T Philips scanner [see fig. 1.4].

Figure 1.4. Philips Intera scanner (3.0 Tesla) at the BCN-Neuro Imaging Center (Groningen, The Netherlands)

1.4. Visual processing

The cornea is a transparent layer, and is the first layer through which the light is passing to the anterior chamber [see fig. 1.5]. The iris controls the amount of light passing to the lens. The ciliary muscle attached to the suspensory ligaments, changes the tension on the lens, controlling the size and shape of the lens. The inner layer is retina containing the photoreceptors (the rods and cones).

The photoreceptors transform the light energy into neurochemical signals. After a number of steps of preprocessing the information, the photoreceptors synapse on the ganglion cells, that are retinal projection neurons, and their axons leave the eye by the optic nerve. Some ganglion cell axons cross at the optic chiasm and go to the contralateral thalamus and brainstem, whereas others remain uncrossed [see fig. 1.6].

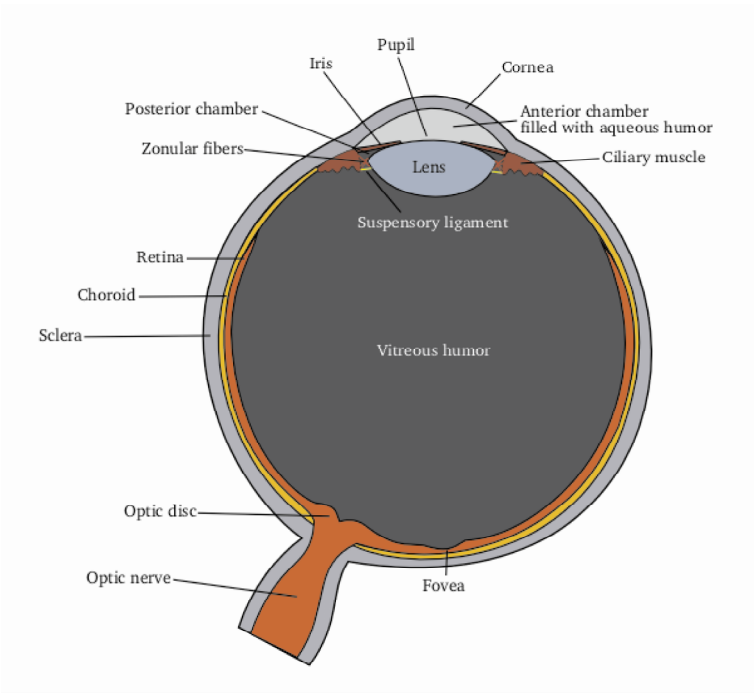

Figure 1.5. Schematic anatomy of the eye (http://en.wikipedia.org/wiki/Eye, 30.01.2007)

The retina projects to four subcortical regions in the brain: the lateral geniculate nucleus, the major subcortical center relaying visual information which projects to the primary visual cortex; the superior colliculus in the midbrain, which controls orienting eye movements; the hypothalamus, which regulates the hormone secretion for the circadian rhythms; and the pretectal nuclei in the midbrain, which control the amount of light reaching the retina in the pupillary reflex.

Substantial visual processing occurs in the occipital lobes of the cerebral cortex. The primary visual cortex is known as V1, Brodmann area 17, or striate cortex. Fibers from V1 project to visual area 2, V2. From V2 some fibers project to visual area 4 (V4), an area specialized for processing color information. There are fibers which project to visual area 5 (V5), or known as mediotemporal cortex where motion and stereo information are processed.

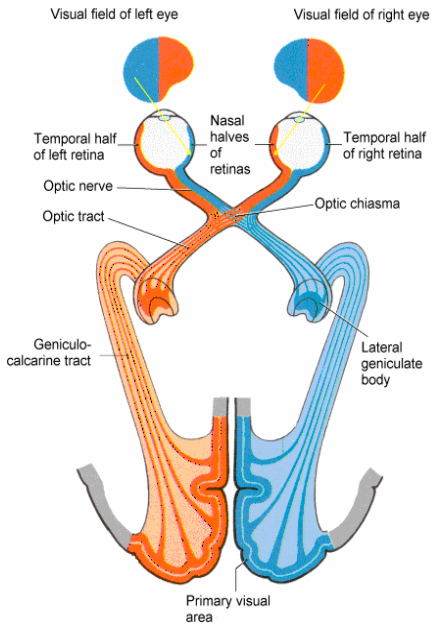

Figure 1.6. Schematic representation of visual pathways: from retina to visual cortex (http://instruct.uwo.ca/anatomy/530/vistopo.gif, 30.01.2007)

1.5. Auditory processing

The human ear can be divided in three distinct areas: the outer, middle, and inner ear [see fig. 1.7].

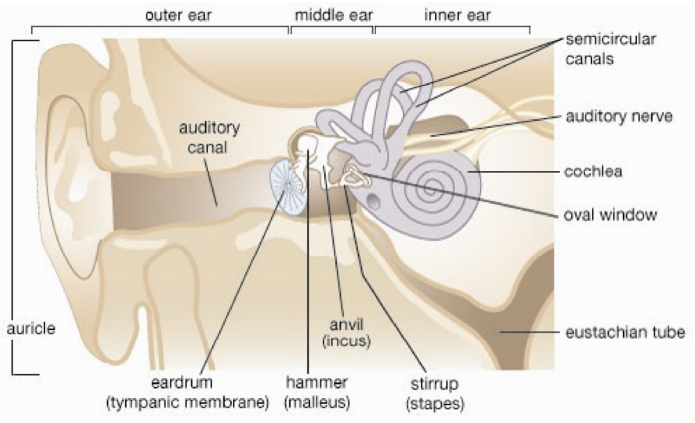

Figure 1.7. Schematic drawing of the peripheral hearing organ (www.concise.britannica.com/ebc/art-66042, 7.02.2003)

Sound is the compression and rarefaction of air, or, an alternating air pressure. Humans can detect sound from 20 Hz to 20 kHz. Sound waves enter the

external ear and through the external auditory canal cause the tympanic membrane to vibrate. The Eustachian tube connects middle ear with the nasal cavity and equalizes atmospheric air pressure inside and outside the tympanic membrane.

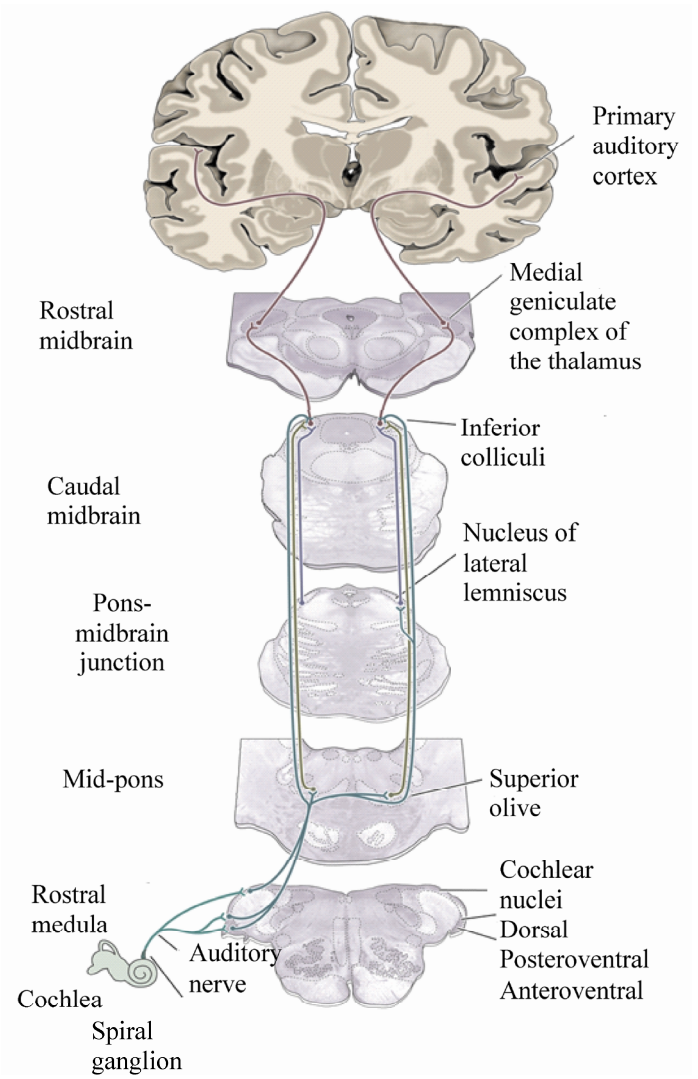

Figure 1.8. A schematic representation of the principal human afferent and efferent auditory pathways (www.rci.rutgers.edu/~uzwiak/AnatPhys, 7.02.2003)

The sound waves that reach the inner ear through the oval window vibrate the perilymph in the scala vestibuli, and the endolymph in the scala media and the scala tympani. Inside of the cochlea, the organ of Corti contains the cells responsible for hearing called hair cells. These cells are attached to the basilar membrane, and the stereocilia or "hairs" from the apical part of the cells are in

contact with the tectorial membrane. Hearing depends on movement of basilar membrane produced by the sound. The high frequencies of the sound waves vibrate the basal part of the basilar membrane, and the low frequencies vibrate the apical end of the membrane. The hair cells are innervated by the bipolar primary sensory neurons located in the spiral ganglion [Martin, 2003].

The nerves from the spiral ganglion terminate in the cochlear nucleus (CN) in the brainstem [see fig. 1.8]. Axons from the neurons in the CN project ipsilateral and controlateral to the superior olive (SO), and controlateral via the lateral lemniscus (LL) to the inferior colliculus (IC). The SO send controlateral fibres to the IC via the LL and efferent fibres to the cochlea. The IC sends the signals to medial genicualte body in the thalamus and from here to the auditory cortex located on the superior surface of the temporal lobe.

The auditory areas consists of primary auditory cortex (Brodmann area 41), second auditory cortex (Brodmann area 42), and higher-order auditory cortex (Brodamnn area 22).

In the next chapter a review of the recent fMRI/MRI studies on the human central auditory pathway is presented.

1.6. References

Bandettini PA, Wong EC, Hyde JS (1992) Time course EPI of human brain function during task activation. *Magn Reson Med* 25(2): 390-7.

Bandettini PA, Jesmanowicz A, Wong EC, Hyde JS (1993) Processing strategies for time-course data sets in functional MRI of the human brain. *Magn Reson Med* 30: 161-173.

Belliveau JW, Rosen BR, Kantor HL, Rzedzian RR, Kennedy DN, McKinstry RC, Vevea JM, Cohen MS, Pykeyy IL, Brady TJ (1990) Functional imaging by susceptibility-contrast NMR. *Magn Reson Med* 14: 538–546.

Belliveau JW, Kennedy DN Jr, McKinstry RC, Buchbinder BR, Weisskoff RM, Cohen MS, Vevea JM, Brady TJ, Rosen BR (1991) Functional mapping of the human visual cortex by magnetic resonance imaging. *Science* 254 (1):716–719.

Casey BJ, de Haan M (2002) Introduction: new methods in developmental science. *Dev Science* 5 (3): 265–267.

Churchland S, Sejnowski TJ (1988) Perspectives on Cognitive Neuroscience. *Science* 242: 741-745.

Duifhuis H (1973) Consequences of peripheral frequency selectivity from nonsimultaneous masking, *J Acoust Soc Am* 4, 1471-1488.

Eden GF, Joseph JE, Brown HE, Brown CP, Zeffiro TA (1999) Utilizing hemodynamic delay and dispersion to detect fMRI signal change without auditory interference: the behavior interleaved gradients technique. *Magn Reson Med* 41:13–20.

Edmister WB, Talavage TM, Ledden PJ, Weisskoff R M (1999) Improved auditory cortex imaging using clustered volume acquisitions. *Hum Brain Mapp* 7: 89–97.

Haacke EM, Brown RW, Thompson MR, Venkatesan R (1999) *Magnetic resonance imaging: physical principles and sequence design*. Wiley. New York.

Hall DA, Haggard MP, Akeroyd MA, Palmer AR, Summerfield AQ, Elliott MR, Gurney E, Bowtell RW (1999): Sparse Temporal Sampling in Auditory fMRI. *Hum Brain Mapp* 7: 213-223.

Hoiting GJ (2005) *Measuring MRI noise*. PhD thesis. University of Groningen.

Liang ZP, Lauterbur PC (2000) Principles of Magnetic Resonance Imaging, *IEEE Press*, New York.

Martin JH (2003) *Neuroanatomy: text and atlas*. 3rd ed. Stamford: Appelton and Lange Stamford. Connecticut.

Ogawa S, Lee TM, Kay AR, Tank DW (1990) Brain Magnetic Resonance Imaging with Contrast Dependent on Blood Oxygenation. *Proc Natl Acad Sci USA* 87: 9868-9872.

Ogawa S, Tank DW, Menon R, Ellermann JM, Kim S-G, Merkle H, Ugurbil K (1992) Intrinsic Signal Changes Accompanying Sensory Stimulation: Functional BrainMapping With Magnetic Resonance Imaging. *Proc Natl Acad Sci USA* 89: 5951-5955.

Ogawa S, Menon RS, Tank DW, Kim S-G, Merkle H, Ellermann JM, Ugurbil K (1993) Functional Brain Mapping by Blood Oxygenation Level-Dependent Contrast Magnetic Resonance Imaging: A Comparison of Signal Characteristics with a Biophysical Model. *Biophys J* 64(3): 803-812.

Ravicz ME, Melcher JR, Kiang NYS (2000) Acoustic noise during functional magnetic resonance imaging. *J Acoust Soc Am*. 108:1683–1696.

Renken R (2004) *Topics in auditory fMRI analysis: - motion - REST - auditory perception and brain response* -. PhD thesis. University of Groningen.

Shah NJ, Steinhoff S, Mirzazade S, Zafiris O, Grosse-Ruyken ML, Jäncke L, Zilles K (2000) The Effect of Sequence Repeat Time on Auditory Cortex Stimulation During Phonetic Discrimination. *Neuroimage* 12: 100-108.

Talavage TM, Edmister WB, Ledden PJ, Weisskoff RM (1999) Quantitative Assessment of Auditory Cortex Responses Induced by Imager Acoustic Noise. *Hum Brain Mapp* 7: 79-88.

Tank DW, Ogawa S, Ugurbil K (1992) Mapping the brain with MRI. *Brain Imaging* 2(10): 525-528.

Turner R, Bihan DL, Moonen CTW, Despres D, Frank J (1991) Echo-planar time course MRI of cat brain oxygenation changes. *Magn Reson Med* 22: 156-166.

Tomaskovic S (2006) *Auditory processing and audiovisual integration revealed by combining psychophysical and fMRI experiments*. PhD thesis. University of Groningen.

Ulmer JL, Biswal BB, Yetkin FZ, Mark LP, Mathews VP, Prost RW, Estkowski LD, McAuliffe TL, Haughton VM, Daniels DL (1998) Cortical activation response to acoustic echo planar scanner noise. *J Comput Assist Tomogr* 22: 111–119.